Supplementary Information

Smartphone assisted high-performance fluorescent colorimetric dual-mode enantioselective identification of glutamic acid in complex samples

Cancan Lu[a], Chen Liu[a], Yaning Duan[a], Tao Yi[b], Cuiling Ren[a,*], Hongli Chen[a]

a State Key Laboratory of Natural Product Chemistry, College of Chemistry and Chemical Engineering, Lanzhou University, Lanzhou, PR China.

b School of Chinese Medicine, Hong Kong Baptist University, Hong Kong Special Administrative Region, PR China

*Corresponding Author

E-mail: rencl@lzu.edu.cn;

Table of contents

1. Chemicals and apparatus

N, N-Dimethyl-phenylenediamine was purchased from Aladdin's Reagent Co. Ltd (Shanghai, China). 3,5-Diaminobenzoic acid (DABA) and the enantiomers of the chiral reagents used (Glutamic acid (Glu), Glutamine (Gln), Arginine (Arg), Histidine (His), Methionine (Met), Proline (Pro), Tryptophan (Trp), Valine (Val), Alanine (Ala), Threonine (Thr), Cysteine (Cys), Asparagine (Asn), Aspartic acid (Asp), Leucine (Leu), Phenylalanine (Phe), Serine (Ser), Lysine (Lys), Norleucine (Nle), Isoleucine (Ile) and Glycine (Gly)) were purchased from Adamas. Hydrogen peroxide, Tris, HCl, NaCl, $CaCl_2$, $CuCl_2$, $AlCl_3$, $FeCl_3$, $MgCl_2$, $MnCl_2$, $ZnCl_2$, NH_4Cl, GSH, Na_2SO_4, Na_2CO_3, $NaHCO_3$, Na_3PO_4, NaAc, $ZnAc_2$, $Na_4P_2O_7$, Na_2SO_3 and other reagents were purchased from Beijing Chemical Reagent Co Ltd (Beijing, China). All chemical reagents were analytically pure and were not further processed before use. Deionized water was used in all experiments.

The TU-1901 dual-beam UV-Vis spectrophotometer was used to measure the UV-Vis absorption spectra of solutions. An RF-5301 fluorescence spectrometer equipped with a xenon lamp was used to scan solutions for fluorescence signals. Circular dichroism (CD) spectra were recorded using the J1500 Circular Dichroism Spectrometer (JASCO, Japan). An Axis Supra spectrometer (Shimadzu, Japan) was used to measure X-ray electron spectroscopy (XPS) and VB-XPS. A time-correlated single-photon counting spectroscopy (TCSPC)-steady-state/transient fluorescence spectrometer (FL920P) was used to determine fluorescence lifetimes. An infrared spectrometer (Nicolet Nexus 670) was used for scanning Fourier transform infrared spectroscopy (FT-IR). JEM-2100 (JEOL, Japan) Transmission electron microscope (TEM) was used to characterize the morphological features and particle sizes of N-NCDs.

2. Calculation

2.1 Fluorescent lifetime

Fluorescent lifetime values of as-prepared samples were calculated by the following formula:

$$\tau_{avg} = \frac{A_1\tau_1^2 + A_2\tau_2^2 + A_3\tau_3^2}{A_1\tau_1 + A_2\tau_2 + A_3\tau_3}$$

Where A_1, A_2, and A_3 are the contribution fractions of the time-resolved decay lifetimes τ_1, τ_2, and τ_3.

2.2 Limit of detection

We calculated the limit of detection (LOD) according to the following formula:

$$LOD = 3\sigma/k$$

The blank measurements' standard deviation (σ) was obtained by fluorescence responses (three times consecutive scanning). Therefore, the limit of detection was calculated by using 3σ/k, σ as the standard deviation, and k as the slope).

2.3 Stern-Volmer constant (K_{SV})

Based on present knowledge, fluorescence quenching arises from static quenching or dynamic quenching. To deeply comprehend the fluorescence quenching, K_{sv} could be obtain from the Stern-Volmer equation：

$$F_0/F = 1 + K_{SV}[Q] = 1 + K_q\tau_0[Q]$$

where [Q] is the concentration of the quencher, K_{SV} is the Stern–Volmer quenching constant, Kq is the dynamic bimolecular burst rate constant controlled by diffusion processes. τ_0 is the average lifetime of a fluorescent molecule in the absence of a bursting agent, and F_0 and F are the fluorescence intensities in the absence and presence of the quencher, respectively.

2.4 Orbital energy levels

The calculation of orbital energy levels includes the HOMO orbital, LUMO orbital, and the band gap (Eg). In this process, VB-XPS is used to determine the HOMO energy, the Tauc method is employed to obtain Eg, and the LUMO energy is calculated as $E_{LUMO} = E_{HOMO} + E_g$.

E_g formula: $\alpha h\nu^{1/m} = B(Hv - Eg)$

Where α is the absorption coefficient, h is Planck's constant, ν is the frequency, B is a constant, Eg is the semiconductor band gap energy, and the exponent n is directly related to the type of semiconductor: n = 1/2 for a direct band gap and n = 2 for an indirect band gap.

3. Experimental section

3.1 Stability testing

N-NCDs were added into buffers with different concentrations of NaCl and pH to study their ionic strength stability and pH stability. The fluorescence intensity of the N-NCDs was measured by incubating at different temperatures to study its thermal stability, and the resistance to photobleaching was determined by irradiating them for 60 min under the excitation light of 365 nm. And exposure to air for a period of time to study the stability of N-NCDs.

3.2 Selectivity and anti-interference experiments

The specific selectivity of N-NCDs was evaluated by adding other interferences instead of Glu. These interferences included some common ions such as Zn^{2+}, Na^{+}, Ca^{2+}, Cu^{2+}, Fe^{3+}, Mg^{2+}, Mn^{2+}, Zn^{2+}, NH_4^{+}, Cl^{-}, SO_4^{2-}, CO_3^{2-}, HCO_3^{-}, PO_4^{3-}, Ac^{-}, SO_3^{2-}, and common amino acids such as Arg, His, Met, Pro, Trp, Val, Ala, Thr, Cys, Asn, Asp, Leu, Phe and Ser. In addition, the interference substances were dispersed in amino acid solution to investigate the anti-interference performance of N-NCDs. The concentration of Glu was 5 mM, the concentration of other amino acids was 10 mM, and the concentration of common ions was 3.3 mM.

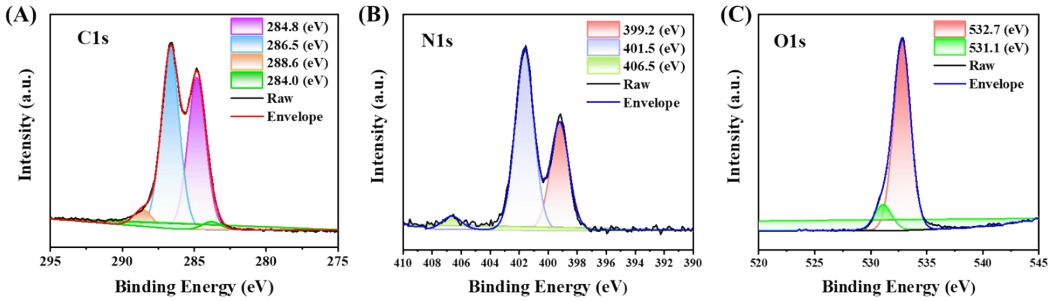

Fig. S1 High-resolution XPS spectra of **(A)** C1s, **(B)** N1s, **(C)** O1s of N-NCDs.

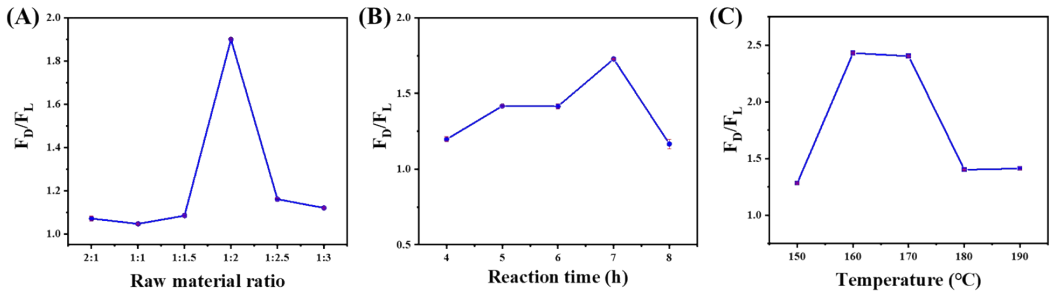

Fig. S2 The effect of **(A)** molar ratio of reactants (N, N-Dimethyl-phenylenediamine: 3,5-Diaminobenzoic acid), **(B)** reaction time, **(C)** reaction temperature on the chiral recognition ability of the synthesized N-NCDs (F_D is the signal value after adding D-AA, F_L is the signal value after adding L-AA)

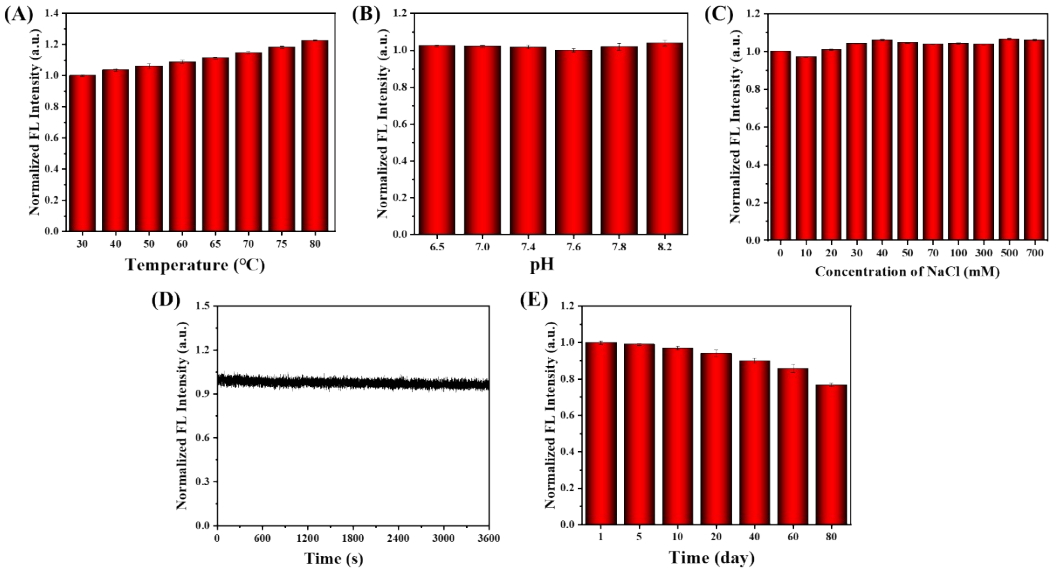

Fig. S3 Changes in fluorescence intensity of N-NCDs at different **(A)** temperatures, **(B)** pH values, **(C)** NaCl concentrations, **(D)** illumination times, and **(E)** time.

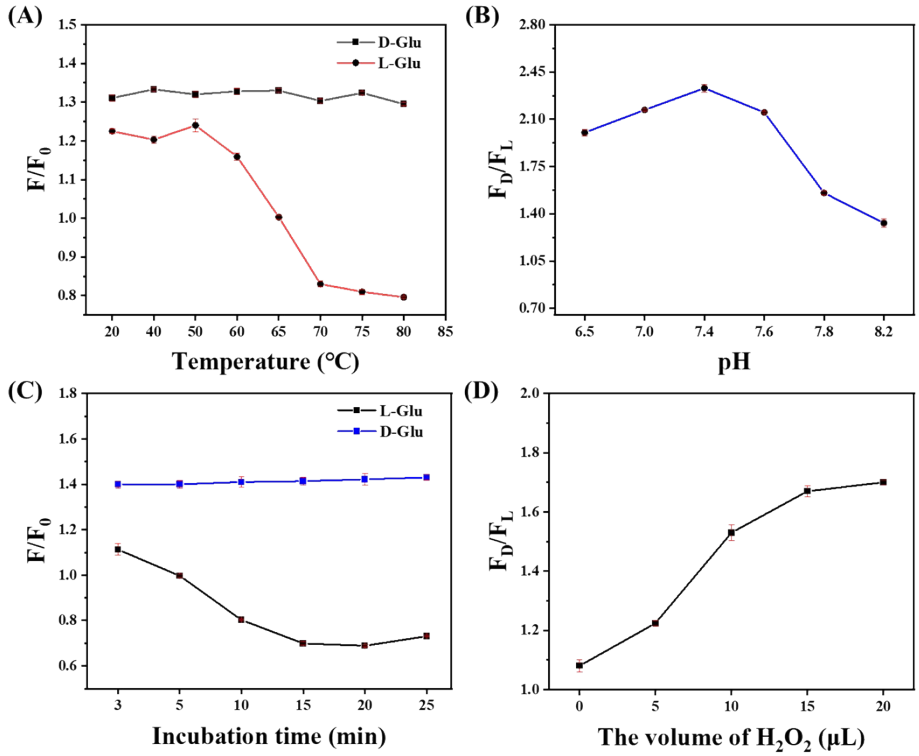

Fig. S4 Fluorescence response of N-NCDs to D/L-Glu at different reaction condition **(A)** temperature, **(B)** pH, **(C)** incubation time, **(D)** H_2O_2 volume.

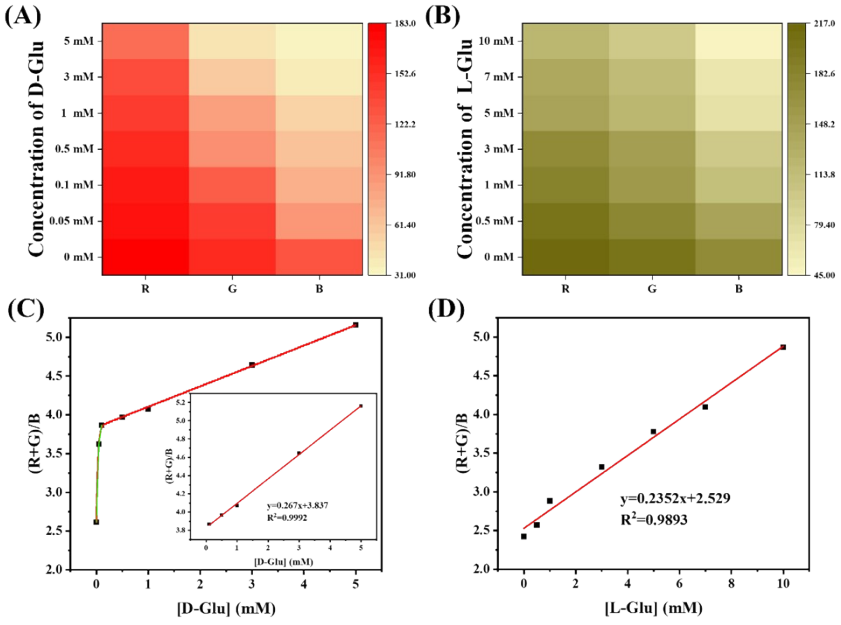

Fig. S5 Heat map derived from the RGB value for **(A)** D-Glu and **(B)** L-Glu, Corresponding color change ((R+G)/B) versus the concentration of **(C)** D-Glu and **(D)** L-Glu

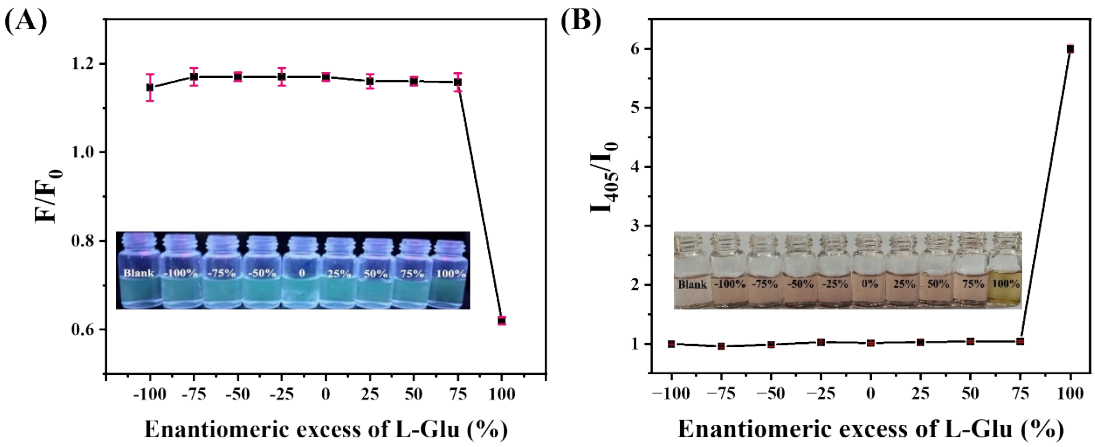

Fig. S6 Relationship between **(A)** F/F_0 and **(B)** I/I_0 with the ee of L-Glu, inset: photographs under **(A)** UV lamps and **(B)** sunlight (D/L-Glu: 5 mM).

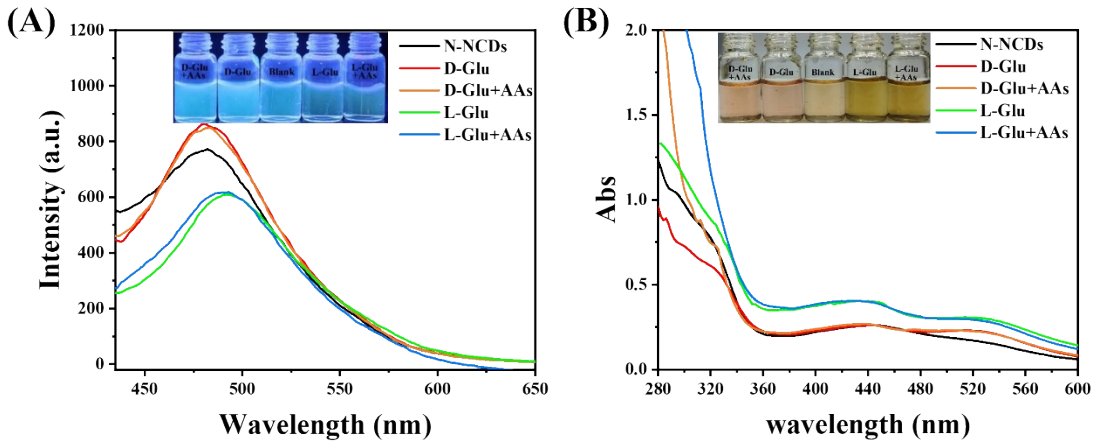

Fig. S7 (A) Fluorescence and **(B)** UV-Vis absorption spectra of N-NCDs at different molar ratios of N-NCDs, D/L-Glu, and D/L-Glu in the 19 kinds of AAs.

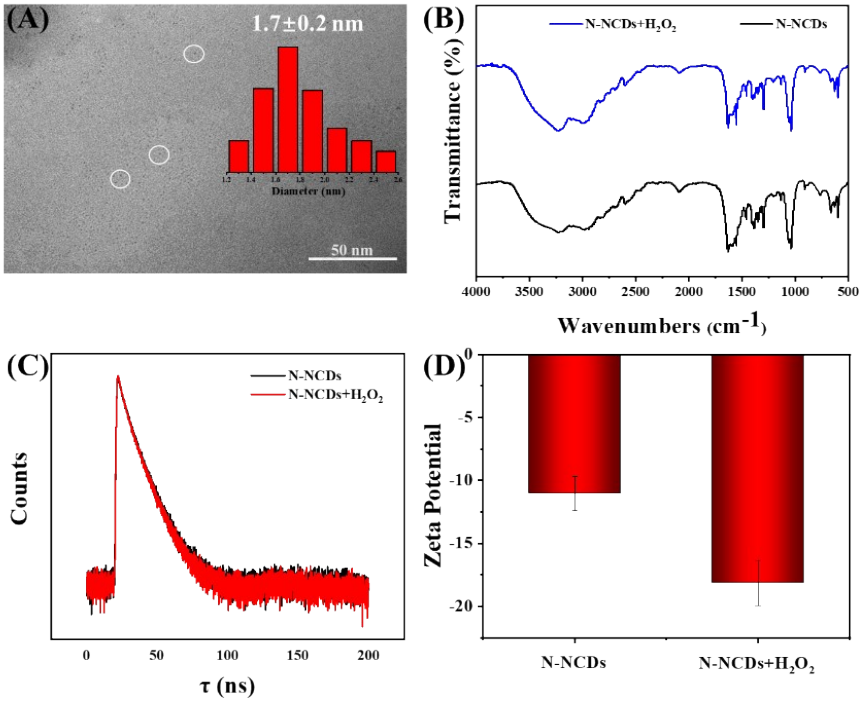

Fig. S8 (A) TEM image of N-NCDs +H_2O_2 (inset: size distributions), **(B)** FT-IR spectra, **(C)** Decay time and **(D)** zeta potential of N-NCDs after addition of H_2O_2.

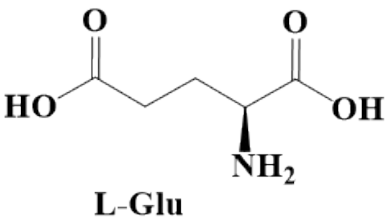

Fig. S9 L-Glu structural formula

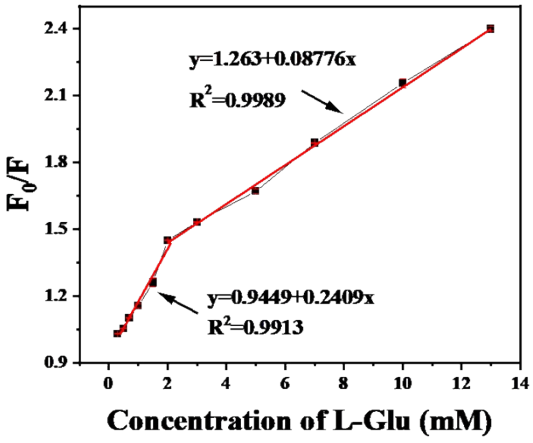

Fig. S10 Relative fluorescence intensity from the quenching of N-NCDs by L-Glu

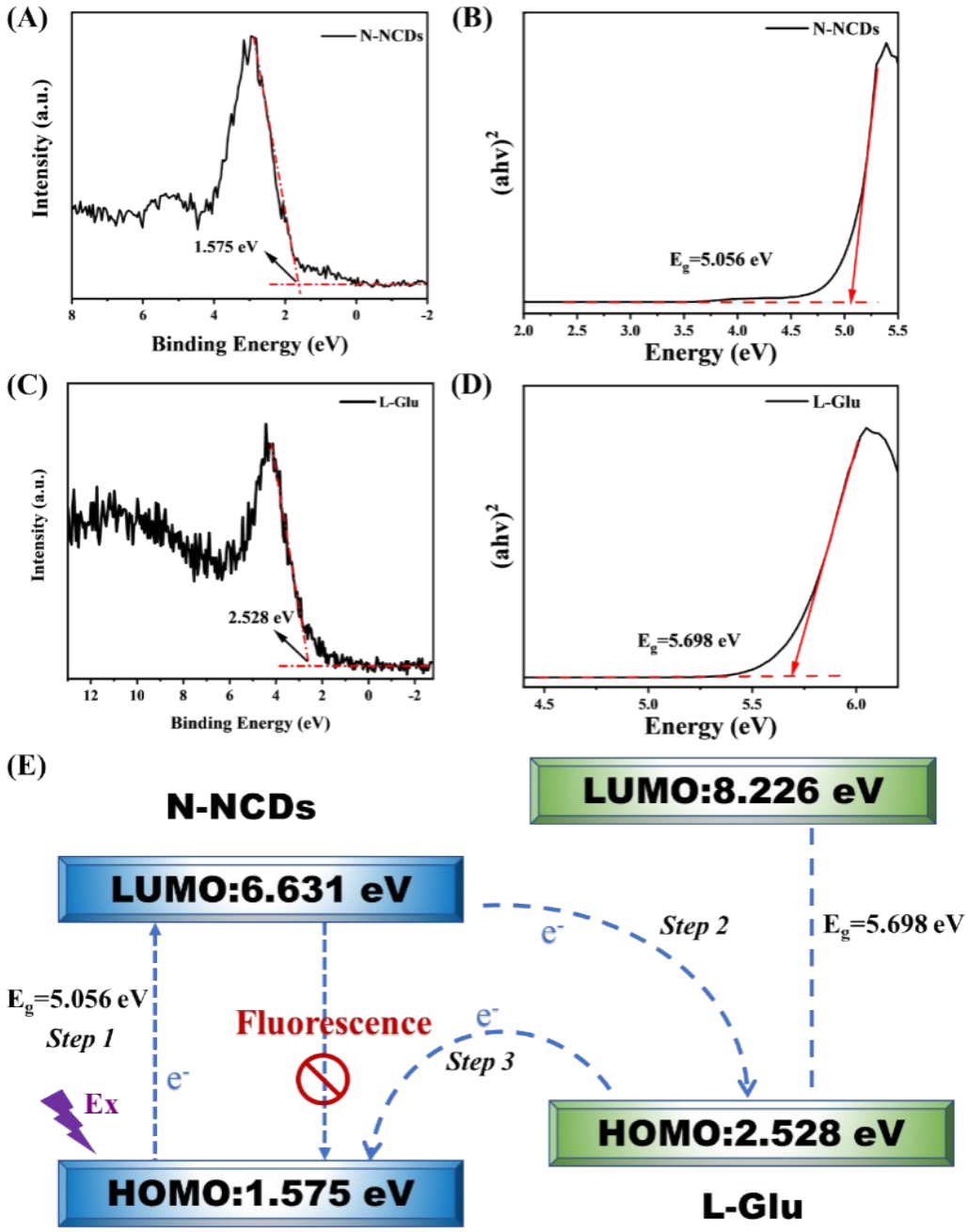

Fig. S11 (A) VB-XPS spectra and (B) Tauc plot of N-NCDs, (C) VB-XPS spectra and (D) Tauc plot of L-Glu, (E) Proposed sensing mechanism of N-NCDs to L-Glu.

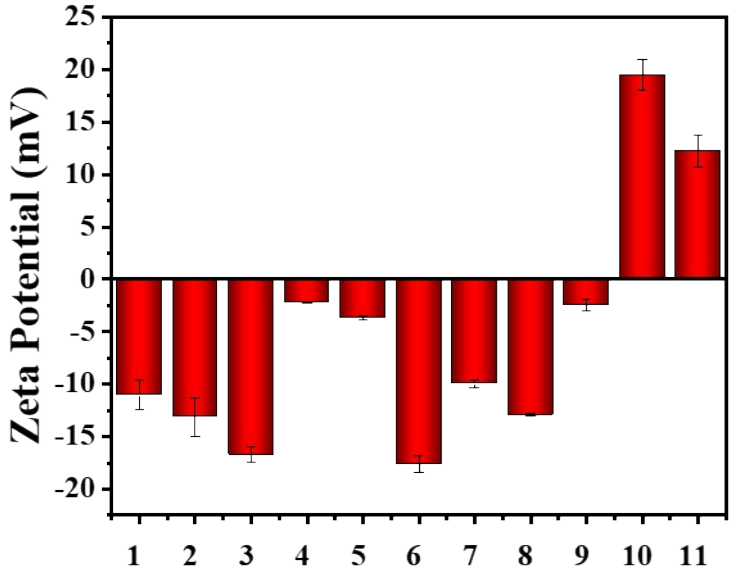

Fig. S12 Zeta potential of N-NCDs after the addition of other amino acids: **1** N-NCDs, **2** Asn, **3** Arg, **4** Leu, **5** Ser, **6** Cys, **7** His, **8** Phe, **9** Asp, **10** L-Glu, **11** D-Glu

4 Possible mechanisms for Gln enantiomers detection

The addition of D-Gln also elevated the fluorescence of N-NCDs, and the mechanism was investigated as hydrogen bond-induced emission (HBIE). As shown in Fig. S13, the particle size is significantly increased by the addition of D-Gln, and the FT-IR spectra show a double absorption peak at 3500 cm^{-1}, which is caused by the difference in N-H vibrational frequencies of $-NH_2$ [1]. Because D-Gln contains $-CONH_2$ and more N atoms (Fig. S14), these functional groups facilitate the uniform distribution of electrons throughout the p-π electron effect and the π-π electron effect, thereby rendering the system more electron-rich, resulting in the zeta potential becoming more negative (Fig. S13D). Consequently, the reaction of the N-NCDs with D-Gln via the conformational rigidity of hydrogen bonding and effective intramolecular and intermolecular spatial conjugation resulted in a more pronounced fluorescence emission following the reaction of N-NCDs with D-Gln [2, 3].

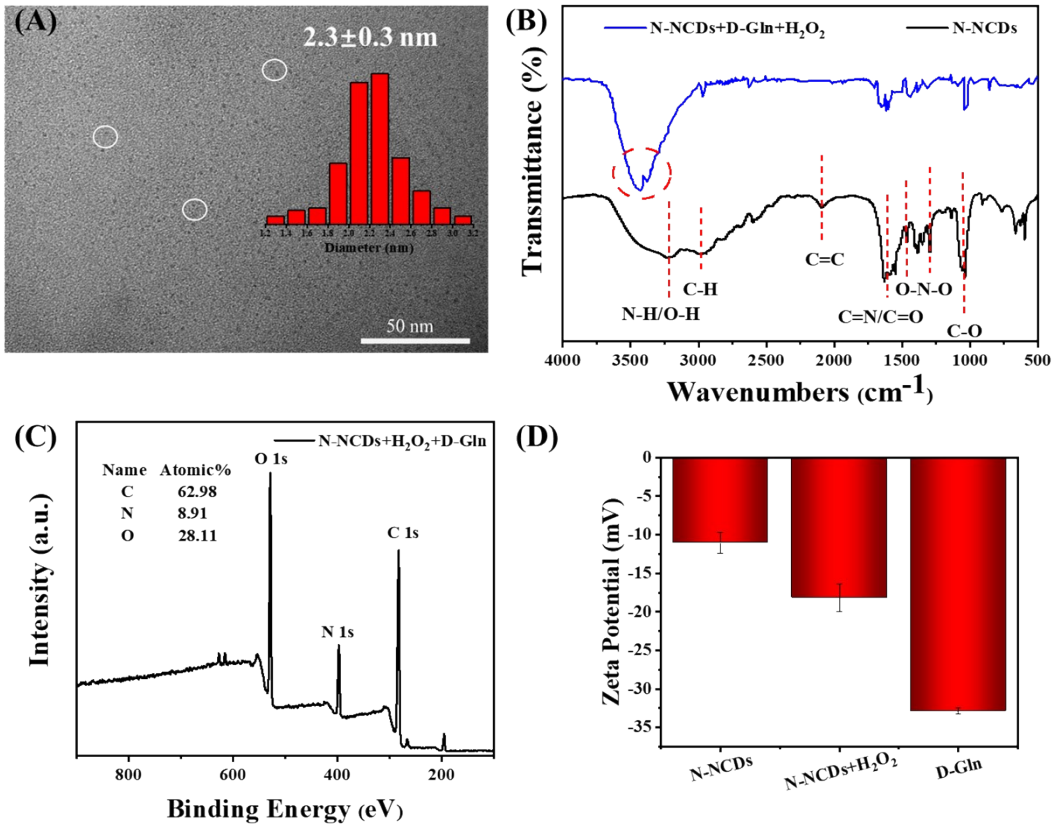

Fig. S13 (A) TEM image, **(B)** FT-IR spectra, **(C)** XPS spectra and **(D)** zeta potential of N-NCDs after the addition of H_2O_2 and D-Gln

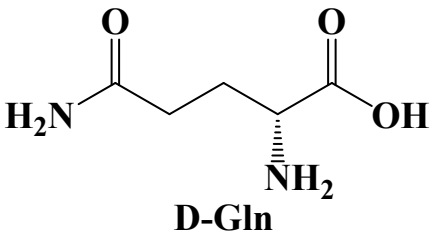

Fig. S14 D-Gln structural formula

Table S1 Comparison of recognition condition parameters for Glu and Gln.

Amino Acid	$V_{N\text{-}NCDs}$ (μL)	$V_{H_2O_2}$ (μL)	Incubation time (min)	Temperature (℃)
D-Glu	70	15	0	20 (R.T.)
L-Glu	90	15	15	70
D-Gln	90	15	15	70
L-Gln	90	15	15	70

Table S2. The detection performance of N-NCDs to AAs enantiomers in fluorescent and colorimetric mode

	Fluorescent mode				**Colorimetric mode**			
Amino Acid	Measurable range (mM)	LOD (μM)	RSD (%)	F_D/F_L	Measurable range (mM)	LOD (μM)	RSD (%)	I_L/I_D
D-Glu	0.05-13	7.28	0.044	3.66	0.03-13	4.83	0.499	7.68
L-Glu	0.3-13	22	0.630		0.1-13	0.97	0.122	

Table S3. Comparison of this work with other reported works for Glu determination.

Recognition methods	Chiral sensor	Enantio-selectivity	Incubation speed (min)	Recognition range (μM)	LOD (μM)	Ref.
Fluorescent	Ga-CDs	Yes	20	D:150-1500	3.90	[4]
Colorimetric				D:150-1500	40.5	
Electrochemistry	Nanostructured porous gold	No	20	50-700	6.82	[5]
Biosensor	Screen-printed microchip	No	/	L:50-1100	35.0	[6]
Fluorescent	Metal Organic Frameworks	No	30	5- 2000	3.0	[7]
Fluorescent	N-GQD	No	15	L:0-1360	15.0	[8]
Fluorescent	2-hydroxy-5-methyl-1,3-benzenedialdehyde	No	0.2	0.5-10	0.64	[9]
Colorimetric				5-35	4.17	
Fluorescent	N-NCDs	Yes	D: 0 L: 15	D: 50-13000 L:300-13000	D:7.28 L:22	This Work
Colorimetric			D: 0 L: 15	D:30-13000 L:100-13000	D:4.83 L:0.97	

/ stands for not provided

Table S4. Determination of Glu in serum and glutamic acid tablets samples (n = 3).

Analyte	Real sample	Recognition methods	Spiked (mM)	Found (mM)	Recovery (%)	RSD (n=3) (%)	Linear regression equations
D-Glu	Diluted serum	Fluorescence method	0	ND	/	/	/
			0.10	0.109	109	1.53	y=0.1119x+1.003 R^2=0.9860
			0.50	0.516	103	1.04	
			1.00	0.980	98.0	2.72	
		Colorimetric method	0	ND	/	/	/
			0.10	0.109	109	1.12	y=-3.049x+9.750 R^2=0.9860
			0.50	0.487	97.4	2.88	
			1.00	0.995	99.5	1.41	
L-Glu	Glu tablet	Fluorescence method	0	0.967	96.7	4.05	y=-0.1615x+0.9982 R^2=0.9925
			0.5	1.487	98.7	1.70	
			1.0	2.009	100.9	2.33	
			1.5	2.558	105.8	1.34	
		Colorimetric method	0	1.022	102.2	2.87	y=3.067x+1.002 R^2=0.9895
			0.5	1.502	100.4	4.12	
			1.0	2.073	107.3	1.34	
			1.5	2.578	105.2	1.56	

ND: Not detected.

/ stands for not provided

References

1. GhaediH, Kalhor P, Zhao M, Clough PT, Anthony EJ, Fennell PS, Potassium carbonate-based ternary transition temperature mixture (deep eutectic analogues) for CO_2 absorption: Characterizations and DFT analysis. Frontiers of Environmental Science & Engineering. 2021; 16 (7): 92.
2. LiQJ, Wang XY, Huang QS, Li Z, Tang BZ, Mao S, Molecular-level enhanced clusterization-triggered emission of nonconventional luminophores in dilute aqueous solution. Nat Commun. 2023; 14 (1):409.
3. Ma LW, Ding BB, Yuan ZY, Ma X, Tian H, Triboluminescence and Selective Hydrogen-Bond Responsiveness of Thiochromanone Derivative. ACS Mater Lett. 2021; 3 (9): 1300-6.
4. Wei SS, Liu BQ, Shi XY, Cui SF, Zhang HY, Lu PJ, Guo H, Wang B, Sun GY, Jiang CH, Gadolinium (III) doped carbon dots as dual-mode sensor for the recognition of dopamine hydrochloride and glutamate enantiomers with logic gate operation. Talanta. 2023; 252:123865.
5. Cai T, Shang K, Wang X, Qi X, Liu R, Wang X, Integration of Glutamate Dehydrogenase and Nanoporous Gold for Electrochemical Detection of Glutamate. Biosensors. 2023; 13 (12): 1023.
6. Yang L, Bai R, Xie B, Zhuang N,Lv Z, Chen M, Dong W, Zhou J, Jiang M, A biosensor based on oriented immobilization of an engineered l-glutamate oxidase on a screen-printed microchip for detection of l-glutamate in fermentation processes. Food Chem. 2023; 405: 134792.
7. Zhang Z, Bai L, Tian H, Han J, Li K, Li Z, Liu Q, Hydrogen-bond induced enhanced fluorescence sensing of metal organic frameworks for colorimetric l-glutamic acid and l-aspartic acid detection. Microchem J. 2025; 208: 112511.
8. Han T, Huang Y, Gao T, Xia C, Sun C, Xu W, Wang D, Fabrication of nitrogen-doped graphene quantum dots based fluorescent probe and its application for simultaneous, sensitive and selective detection of umami amino acids. Food Chem. 2023; 404: 134509.
9. Li M, Li SZ, Huang Y, Dong WK, A dual-channel chemosensor based on 2-hydroxy-5-methyl-1,3-benzenedialdehyde for fluorescence detection and colorimetric recognition of glutamic acid. Journal of Photochemistry and Photobiology A: Chemistry. 2022; 431: 114053.